Chaos, Solitons and Fractals xxx (xxxx) xxx

Contents lists available at ScienceDirect

Chaos, Solitons and Fractals

Nonlinear Science, and Nonequilibrium and Complex Phenomena

journal homepage: www.elsevier.com/locate/chaos

Exploiting the impact of ordering patterns in the Fisher-Shannon complexity plane

David Spichak, Andrés Aragoneses*

Physics department, Eastern Washington University, Cheney, 99004, WA, USA

ARTICLE INFO

Article history:
Received 11 August 2021
Revised 1 October 2021
Accepted 1 November 2021

Keywords:
Chaos
Complex systems
Permutation entropy
Fisher information measure
Determinism
Stochasticity
Non-invertible maps

ABSTRACT

The Fisher-Shannon complexity plane is a powerful tool to characterize complex dynamics. It locates, on a two-dimensional plane, a dynamical system based upon its entropy and its Fisher Information Measure (FIM). It has been recently shown that by using ordinal patterns to compute permutation entropy and FIM, this plane unveils inner details of the structure underlying the complex and chaotic dynamics of a system, not easily exposed by other methods. The entropy of the dynamics is invariant to the way the patterns are ordered, but the way FIM is defined is sensitive to the order in which we classify the ordinal patterns. In this paper we analyze in detail the impact that the sorting protocol used to calculate FIM has on the structure unveiled by the Fisher-Shannon plane. We show the importance of a suitable choice, which can lead to saving computational resources, but also to disclose details of the dynamics not accessible to other sorting protocols. Our results agree with previous research, and common characteristic fingerprints are found for the different chaotic maps studied. Our analysis also reveals the fractal behaviour of the chaotic maps studied. We extract some underlying symmetries that allow us to simulate the behaviour on the complexity plane for a wide range of the control parameters in the chaotic regimes.

1. Introduction

Describing and characterizing the complex dynamics of chaotic systems is a challenging task. Some techniques are computationally demanding, and some hidden features of the dynamics are hard to determine. There are several tools in the literature to quantify and characterize chaos. Some can help distinguish stochasticity from deterministic chaos, some allow discrimination among different dynamical regimes in a complex dynamical system [1–5]. Among them, Entropy and Fisher Information Measure (FIM), to be described later, are two quantifiers that extract global and local information, respectively, from a complex system. A convenient way to present these two quantifiers is through the Fisher-Shannon complexity plane [6], that projects the FIM of the system versus its entropy, localizing the dynamics of the system on a two-dimensional plane. Fig. 1 (explained in detail in the next section) presents the entropy versus FIM for the logistic map, $x_{n+1} = rx_n(1 - x_n)$, as the control parameter is scanned from $3.55 \leq r \leq 4.0$.

This technique has shown the ability to characterize nonlinear dynamics, and to distinguish between stochastic noise and deterministic chaos [7–9] by comparing and tracking the locations of dynamical systems on the plane.

In a recent work, Spichak et al. [10] studied the Fisher-Shannon complexity plane of different chaotic iterative maps under the lens of Bandt and Pompe's [11] ordinal patterns approach. They projected the different maps on the plane as they scanned their control parameters. Spichak et al. found that, using ordinal patterns to calculate the Fisher-Shannon plane is more powerful than a more traditional PDF-based Fisher-Shannon analysis, when it comes to unveiling the hidden structure of complex dynamical systems. An interesting feature identified is that most of the non-invertible iterative maps share a common fingerprint on the plane as the control parameter is scanned. Spichak et al. also showed how this technique detects transitions in the dynamical behaviour of the chaotic system.

However, when computing the location of a complex dynamical system on the Fisher-Shannon plane, entropy is invariant to how we order the patterns but FIM is sensitive to the chosen order [8,10]. This can lead one system to be projected in different locations on the plane when using different arrangements of the patterns. In this paper we explore the impact of the sorting protocol of the ordinal patterns in extracting information through the Fisher-Shannon complexity plane.

* Corresponding author.
E-mail address: aaragoneses@ewu.edu (A. Aragoneses).

https://doi.org/10.1016/j.chaos.2021.111620
0960-0779/© 2021 Published by Elsevier Ltd.

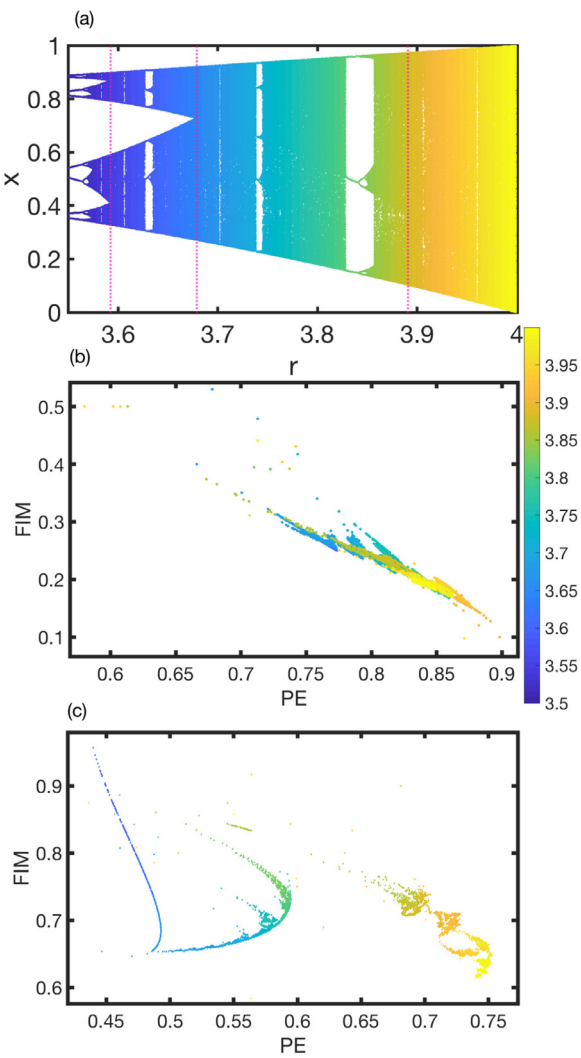

Fig. 1. (a) Bifurcation diagram of the logistic map. Dashed lines indicate where symmetry breaking takes place (explained in the main text). (b) Fisher-Shannon plane for the logistic map using ordinal patterns of dimension $D = 3$. (c) Fisher-Shannon plane for the logistic map using ordinal patterns of dimension $D = 4$. FIM has been computed using Lehmer sorting protocol. 10^4 values of the control parameter are computed in (b) and (c), in the range $3.55 \leq r \leq 4.0$. We use a color scale to identify r in the figures.

2. The Fisher-Shannon plane using ordinal patterns

2.1. Permutation entropy

In order to compute the entropy and FIM of the time series of a complex dynamical system, the ordinal patterns approach transforms the raw time series of the dynamics into a sequence of patterns, also known as *words*. These words are built by comparing consecutive values of the time series [11]. The number of possible words will depend on their dimension, i.e., on how many consecutive values we consider to construct the words. Words are assigned depending on the relative magnitudes of consecutive points in the time series. For example, for dimension $D = 2$ we compare two consecutive values, $\{x_i, x_{i+1}\}$. If $x_i < x_{i+1}$ we assign the word 01. For $x_{i+1} < x_i$ we assign the word 10. Similarly, for dimension $D = 3$, if $x_i < x_{i+1} < x_{i+2}$ then we assign the word 012; if $x_i < x_{i+2} < x_{i+1}$ then we assign the word 021, and so on. We have a total of $D!$ different words for dimension D. These words capture temporal correlations among consecutive values, or events, of the time series. Some experimental time series, because of limited instrumental resolution, or some mathematical models with periodic behaviour, present equal consecutive values ($x_i = x_{i+1}$). In the iterative chaotic maps under consideration that situation does not occur.

From the sequences of patterns we calculate the probability of each word, and we compute the Permutation Entropy (PE) as

$$PE = \frac{1}{ln(D!)} \sum_{i=1}^{D!} p_i \; ln(p_i) \tag{1}$$

where D is the dimension of the words, $D!$ is the number of different possible words, p_i is the probability of the ith word, and PE is normalized so that $0 \leq PE \leq 1$. For a purely random distribution (white noise) PE is maximum, while for a completely regular distribution, where only one word is present and the system is completely predictable, PE is zero.

Permutation entropy is a measure of the global behaviour of the dynamics. This measure is robust to changes in the distribution on small scales, like those coming from experimental noise, or equipment resolution. For example, some small noise added to a triad of values changes the actual values of the events of the time series. Nevertheless, this does not impact the patterns and the computed permutation entropy, as these patterns rely on how they compare to their neighbours: $\{2.25, 3.85, 0.65\} \rightarrow 120$; $\{2.43, 3.70, 0.90\} \rightarrow 120$. Permutation Entropy is also invariant to the way we order the $D!$ words.

This protocol implies a compression of information: words lose the information of the exact values in the time series, but they are able to extract signatures of temporal correlations in the dynamics. This method of calculating the entropy is useful in unveiling long temporal correlations in the dynamics, in identifying time delays, in finding temporal scales, in distinguishing random behaviour from determinism, and in statistically forecasting events [12–18].

2.2. Fisher information measure

Fisher Information Measure (FIM) is another quantifier of complexity. It measures the rate of change of consecutive values in a time series, which makes it sensitive to small, localized changes and perturbations in the values of the time series. For a distribution with N possible values it can be defined as

$$FIM = F_0 \sum_{i=1}^{N-1} \left((x_{i+1})^{1/2} - (x_i)^{1/2} \right)^2 \tag{2}$$

where $F_0 = 1$ if $x_{i^*} = 1$ for $i^* = 1$ or $i^* = N$, and $x_i^* = 0 \; \forall i \neq i^*$. Otherwise $F_0 = \frac{1}{2}$. $\{x_i, \; i = 1, \ldots, N\}$ is the time series. For a purely ordered system FIM is maximum, while for a purely stochastic, uncorrelated process FIM is zero. FIM has been shown to be a powerful tool to identify and characterize complexity in nonlinear dynamical systems [19–22].

PE and FIM complement each other, as the former extracts information about the dynamics at a global scale and can feature long temporal correlations in the time series, while the latter describes the local correlations of the dynamics in the time series. For this reason, the Fisher-Shannon plane is a good tool to characterize complex dynamics, distinguish stochasticity from chaos, and differentiate dynamical regimes. In this paper we compute FIM based on ordinal patterns, where $\{x_i\}$ is replaced by $\{p_i\}$, the probabilities of the words, in Eq. (2).

However, the way FIM is defined entails that the order of the probability distribution set affects the computed FIM. For a given set of N different values with probabilities $\{p_i, \; i = 1, \ldots, N\}$ there are $N!$ possible options of sorting them. Each one of the possible sorting protocols can provide a different value of FIM. Olivares et al. [8] studied the two most common ordering criteria, the Lehmer and Keller sorting protocols, for the logistic map, using

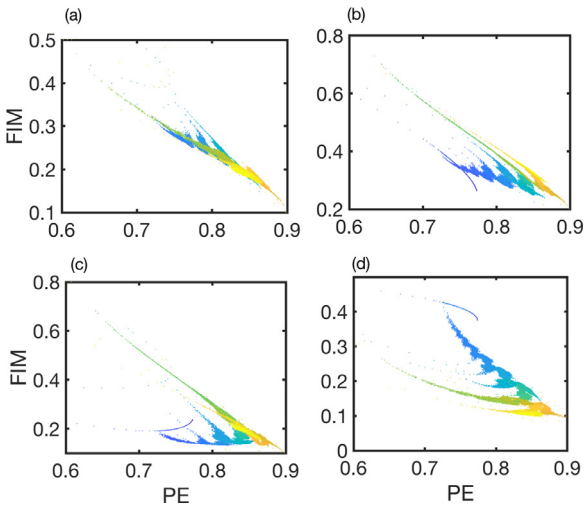

Fig. 2. Fisher-Shannon plane for the logistic map using words of dimension $D = 3$. Four different ordering protocols are presented: (a) Lehmer (SA-123456), (b) Keller (SA-125346), (c) SA† (SA-431652), and (d) SA* (SA-241536). See main text for a description of SA labels. 10^5 values of the control parameter r are computed for each plot, $3.55 \leq r \leq 4$.

words of dimension $D = 6$. For the windows of regularity in the bifurcation diagram of the map, they found that FIM from both ordering criteria coincide, but in the chaotic regions each sorting criteria gives a different FIM. They detected a linear relationship between both criteria for the period doubling regions present in the dynamics, but no clear relationship for more chaotic regions.

For words of dimension $D = 3$ there are $D! = 6$ possible words, and $(D!)! = 720$ possible orders for these words. This large number of possibilities makes a detailed analysis of all possible orders an impossible challenge for dimensions $D \geq 4$. Here we present a detailed analysis of how the ordering criteria for words of dimension $D = 3$ impact the Fisher-Shannon plane.

3. The Fisher-Shannon plane for different sorting criteria

The Fisher-Shannon plane locates the complex dynamical system on a 2D plane. As we scan a control parameter of the system we can track its trajectory on the plane, which allows us to compare the system at different control parameter values and find similarities and differences in its dynamical structure. Values that overlap on the 2D plane can be related to similar dynamical regimes, while values that are far apart on the plane can indicate differences in the dynamics. This can also help identify universality patterns among different dynamical systems [10]. Having the complex system spread out on the 2D plane can help identify detailed features of the system, while having the complex system concentrated in a narrow area can tell us little about its features.

When using words to compute the Fisher-Shannon plane (PE and FIM), because of the nature of the words, we are exploring temporal correlations in the dynamics. Using words of different dimensions can reveal differences in the dynamics at different temporal scales. Higher dimensions can extract longer temporal correlations from the dynamics, or more complex dynamical structures. In the case of Fisher-Shannon plane we can see in Fig. 1 that $D = 4$ portrays a more detailed structure than $D = 3$. Nevertheless, while this increase in detail is obvious for lower dimensions, for words of dimension $D > 5$ the gain in detail becomes less significant (see Fig. 2 from Ref. [10]).

Fig. 1 presents the bifurcation diagram of the logistic map and the Fisher-Shannon plane for words of dimension $D = 3$ and $D = 4$. It is clear how the higher dimension plot presents a more detailed structure, distinguishing regions based upon their dynamics. For example, for dimension $D = 3$ most of the r-values lie on the same region showing low structure, following a straight-line shape on the plane, with blue dots (lower r values) and yellow dots (higher r values) occupying the same area; for dimension $D = 4$ the complexity plane distinguishes different regions as the system deploys a clear structured pattern on the plane as we scan the control parameter r.

It makes sense that higher dimensionality picks up more details of the dynamics, as we are considering more possible words, each one of them extracting a particular aspect of the temporal correlations in the time series. But reordering the words before we compute FIM also has an impact on the level of detail we can extract from the plane. Fig. 2 presents the Fisher-Shannon plane for the logistic map using words of dimension $D = 3$ for four different ways of sorting the words before computing PE and FIM. In it, we can appreciate how different the structure is portrayed. While there is no change in the values of PE across the sorting protocols, FIM does change, which affects the vertical values in the plots.

Fig. 2 a corresponds to the Lehmer sorting protocol, Fig. 2b to Keller, Fig. 2c to SA†, and Fig. 2d to SA* (the labeling of these sorting protocols to be described later). While the FIM range in Fig. 2a, b, and d are comparable, Fig. 2c needs a wider vertical axis to accommodate the dispersion in FIM values for SA†, indicating the suitability of this sorting protocol to differentiate dynamical structures in the system.

Because the quantifiers (PE and FIM) describe the complex dynamics of the system, having the system spread out on the complexity plane helps distinguish different dynamical regions. Also, the structure present on the plane helps identify similarities in the system.

If we look at Fig. 2c, where the control parameter grows from blue to yellow, we can appreciate in it the different regions of the bifurcation diagram of the logistic map (Fig. 1a). A base line at the bottom (blue-green) keeps a similar FIM value (around 0.2) as PE increases (moving to the right, from 0.73 to 0.87). Some branches leave the bottom line, increasing FIM and decreasing PE (move up and left). These branches are directly related to the bifurcation diagram of the map. At each window of periodicity, the dots of the plot sharply escape from the bottom line to the far end of each branch (FIM increases and PE decreases). Then, at the period-doubling routes to chaos, the system increases PE and decreases FIM stepwise, and moves from the far end of each branch to the bottom line. Finally, the system follows the structureless yellow curve as the logistic map explores its most chaotic region and the entropy of the system increases. All of these features can be appreciated in all four sorting protocols, but it is visually more obvious for some of them (SA† and SA*).

In order to differentiate regions that have different dynamical features it would be beneficial to find that sorting protocol that spreads out the chaotic map the most on the plane. This would locate those values of the control parameter for which the dynamical behaviour is similar in nearby regions of the geography of the plane, while separated from those values of the control parameter for which the dynamical behaviour is more different to them.

There are 720 ways of sorting the six words of dimension $D = 3$. In order to label them we follow the next criteria: we assign a number to each one of the six words as

Ordinal pattern	Word label
012	1
021	2
102	3
120	4
201	5
210	6

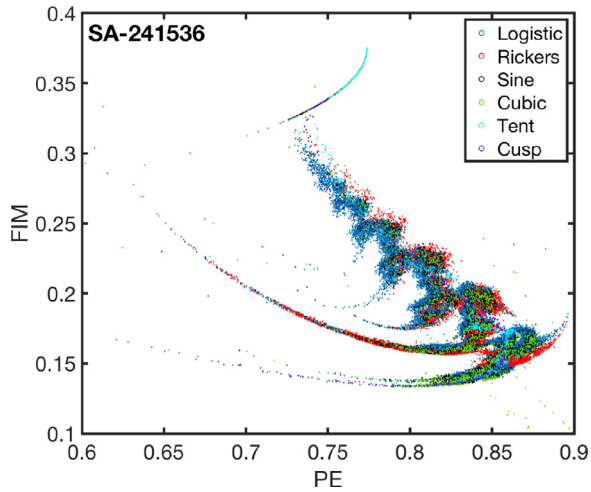

Fig. 3. Fisher-Shannon plane for words of dimension $D = 3$ using SA-241536 (SA^*) for the logistic, Ricker's, sine, cubic, tent, and cusp maps. Just as happened for SA-Lehmer [10], they all share the same fingerprint on the plane. Each map has been computed with 10^4 realizations of r.

Then we assign the sorting array (SA) corresponding to the order of the label of the words to each specific sorting protocol. After this, Lehmer protocol is SA-123456; Keller protocol is SA-125346, and so on:

Lehmer SA-123456	Keller SA-125346	SA* SA-241536	SA† SA-431652
012	012	021	120
021	021	120	102
102	201	012	012
120	102	201	210
201	120	102	201
210	210	210	021

We find that the protocols SA-241536 (SA^*) and SA-431652 ($SA^\dagger$) are especially convenient to see detailed structure (see Fig. 2c and d). These sorting arrays scatter FIM values on the plane, allowing to differentiate the internal features more than most other sorting arrays.

Of all the 720 different sorting arrays there are some for which their projection on the Fisher-Shannon plane coincide. A display of all these sorting arrays for the logistic map can be found in Refs. [23,24]. By visual inspection of them we decide to focus on SA* and SA† as these two sorting arrays present the most detailed structure on the Fisher-Shannon plane.

In a previous work [10], using ordinal patterns and SA-Lehmer, it was found that most non-invertible maps leave the same fingerprint on the Fisher-Shannon plane, even when this fingerprint changes with the dimensionality of the words. This commonality is also present for the other sorting arrays. Fig. 3 shows the Fisher-Shannon plane for the logistic, Ricker's ($x_{n+1} = rx_n e^{-x_n}$), sine ($x_{n+1} = r\ \sin(\pi x_n)$), cubic ($x_{n+1} = rx_n(1 - x_n^2)$), tent ($x_{n+1} - r\ \min\{n_n, 1 - x_n\}$), and cusp ($x_{n+1} = 1 - r\sqrt{|x_n|}$) maps, for SA^*. In it, all maps cover the same region and they feature the same structure, pointing at akin dynamical complexity. As it was found for Lehmer, the tent and cusp maps present a simpler structure that only covers the skeleton of the more complex structure deployed by the other maps. This behaviour is present for other sorting arrays (not shown).

4. Complex structure in the logistic map

As can be seen from Fig. 2a, sorting the words using SA-Lehmer does not extract as much structure as other protocols. On the other hand, when using SA* (see Fig. 2d) the plot for the logistic map covers a wider region on the plane and some recurrent behaviour can also be appreciated. For SA*, the most chaotic values (yellow) do not overlap with the less chaotic ones (blue and green), as happens for SA-Lehmer. There is also a well-defined curve for lower r values (blue in the figure), that is not obvious with SA-Lehmer. This range of r values goes from the onset of chaos ($r = 3.569$) to the merging of the two branches in the bifurcation diagram (at $r = 3.679$). Even though the system is chaotic for these r values, this well-defined curve on the Fisher-Shannon complexity plane is indicating the presence of some internal symmetry in the dynamics.

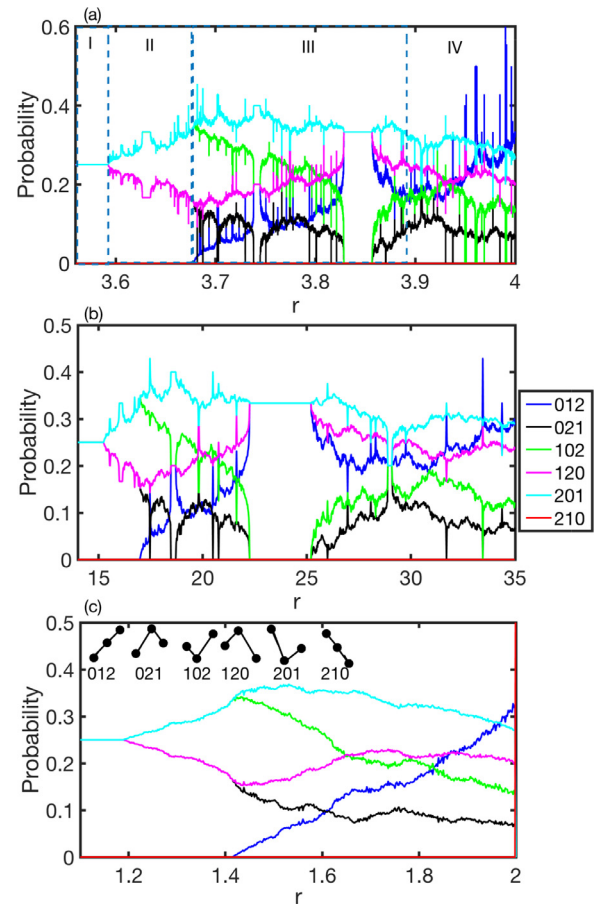

Fig. 4. Words probabilities ($D = 3$) versus control parameter r, for the logistic (a), Ricker's (b), and tent maps (c). In the logistic map (a) three regions are distinguished indicating different internal symmetries in the complex dynamics. In (c) visual representations of the words are depicted.

In order to explore the details of the symmetries on the dynamics in this regime, we plot the probabilities of the six words of dimension $D = 3$ versus the control parameter of each map. Fig. 4 shows those probabilities for the logistic, Ricker's, and tent maps. All three figures share common features as the control parameter is scanned. This general behaviour is also present in other non-invertible maps (not shown).

From Fig. 4 we see that the system starts with high symmetry, portrayed in the words probabilities for all these maps with one cluster of four words. Words 021, 102, 120, and 201 have the same probability, while words 012 and 210 are forbidden (210 is forbidden for the whole range). After that, this high symmetry breaks into a lower symmetry and the cluster splits into two smaller clusters: 021-120 and 102-201. These two clusters then break down so that each word from previous clusters has a different probability, and the word 012 starts to have non-zero probability.

The fact that words are grouped in clusters indicates the presence of determinism and internal symmetries in the dynamics. In each of those regions we can find a correlation among probabilities more restrictive than the default one:

$$P_j = 1 - \sum_{i \neq j} P_i. \tag{3}$$

There are four differentiated chaotic regions in these maps. They are indicated in Fig. 4a with roman numerals for the logistic map:

- Region I ($r < 3.592$) contains one cluster and two forbidden words ($P_1 = P_6 = 0$, $P_2 = P_3 = P_4 = P_5 = \frac{1}{4}$). The system on the complexity plane is fully determined in this range, with a defined value for PE and for FIM.
  Words in this region are grouped so that each word in the cluster is the time inverse of another word in the same cluster (102 → 201, 012 → 210, ...), but they are also the time and intensity inverse of each other (102 → 021, 012 → 012, ...). This indicates that the dynamics present mirror symmetry (temporal reversibility) and rotational symmetry [25]. The term rotational symmetry introduced in Ref. [25] comes from the fact that, by rotating 180 degrees one of the words, as seen in Fig. 4c, we obtain the other word in the cluster.
- Region II ($3.592 < r < 3.679$) contains two clusters and two forbidden words

$$\begin{aligned} &P_1 = P_6 = 0 \\ &P_2 = P_4 \neq P_3 = P_5. \end{aligned} \tag{4}$$

  The system here has one degree of freedom, as we only need to know one of the probabilities to determine all the remaining ones.
  In this region the dynamics presents only mirror (temporal) symmetry, as each cluster is formed by those words that are the time inverse of the each other (012-210; 102-201; 021-120).
- Region III ($3.679 < r < 3.891$) has no clusters and only one forbidden word ($P_6 = 0$). But by visual inspection of the probabilities one can see that the five remaining words are constrained by the following correlations:

$$\begin{aligned} &P_2 = \tfrac{1-3P_1}{2} - P_3 \\ &P_4 = P_1 + P_2 \\ &P_5 = P_1 + P_3. \end{aligned} \tag{5}$$

  The probabilities are not fully independent. The system here has two degrees of freedom. We only need to determine the probabilities of two words (for example P_1 and P_3) to determine its unique position on the complexity plane.
- In region IV ($3.891 < r \leq 4.0$) we have not found constraints in the probabilities, other than that of Eq. (3) and $P_6 = 0$. The probabilities are not related.

This differentiation of regions is a general feature found also for the other non-invertible maps under consideration. The dotted lines in Fig. 1a indicate the r-values where there is a symmetry breaking for the case of the logistic map. Two of them ($r = 3.592$ and $r = 3.679$) can be related to the merging of two wide regions in the bifurcation map. The third one is not obvious. If we zoom in the $r = 3.891$ region (see Fig. 5) we can see that there is another merging-like behaviour at this value, although the bifurcation diagram is much more complex here, and the dynamics much less restrictive.

Because of these correlations found in the different regions, we can simulate the Fisher-Shannon complexity plane without using the iterative equation of any specific map. All the maps that contain these relations among words probabilities (Eqs. (4), (5)) should lie on the same region and they should present the same fingerprint on the plane. We compute PE and FIM using the probabilities

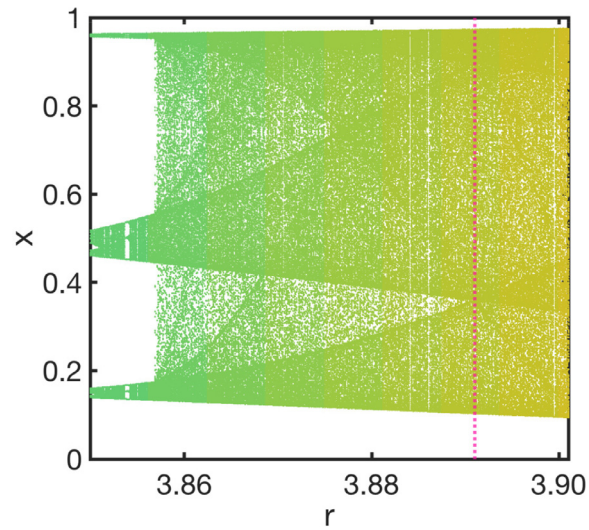

Fig. 5. Bifurcation diagram for the Logistic map around the third symmetry breaking, $r = 3.891$, indicated by the dotted line.

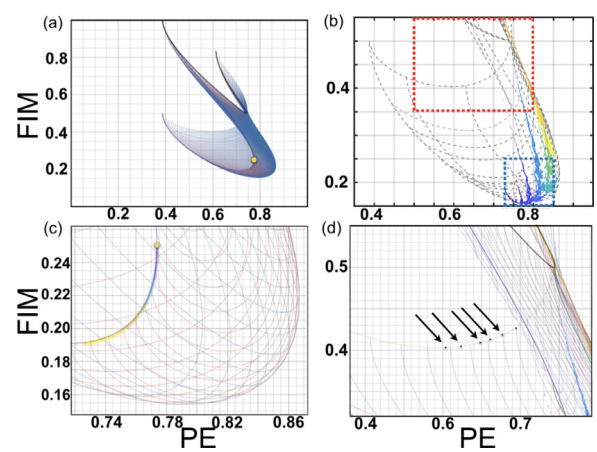

Fig. 6. (a) Numerical simulation of the complexity plane using the underlying constraints (Eqs. (4) and (5)), for SA† and $D = 3$. Yellow dot indicated the only allowed position for the logistic map in region I. (b) Logistic map (in color) is shown overlapped with the numerical simulation (in gray). (c) Zoom in of the blue dashed rectangle from (b). Regions I and II for the logistic map are also shown overlapped with the numerical simulation. (d) Zoom in of the red dashed rectangle from (b). Arrows indicate the dots corresponding to the windows of periodicity in the logistic map in regions II and III, which lie on top of one of the boundaries of the simulation. (For interpretation of the references to colour in this figure legend, the reader is referred to the web version of this article.)

given by Eqs. (3), (4), and (5), instead of using any of the iterative maps under study.

For region I, because the probabilities are fixed by $P_2 = P_3 = P_4 = P_5 = \frac{1}{4}$, there is only one option for PE and for FIM (for SA†, PE=0.7737 and FIM=0.25). This means that all this region is described by a single dot on the plane. Fig. 6 shows the numerical simulations to re-create the landscape on the Fisher-Shannon plane. The yellow dot in Fig. 6a, c indicates the only allowed position for region I. The position of this dot is different for different sorting arrays (SA), but it coincides for some of them.

For region II we have a richer behaviour, that allows for several combinations to satisfy that $P_2 = P_4 \neq P_3 = P_5$. We scan $0 \leq P_2 = P_4 \leq \frac{1}{2}$ and $P_3 = P_5 = \frac{1}{2} - P_2$, obtaining all PE and FIM allowed values, and therefore, all allowed projections on the complexity plane under Eq. (4). For this constraint, the system leaves the dot on the FIM-PE plane in Fig. 6a and starts to explore other values on the plane. We obtain the well defined curved line starting at the dot

that described region I. Fig. 6c shows the curved line for the logistic map (blue to yellow line) superimposed on the curve defined by our simulations. This curved line defines the allowed values for region II of the different chaotic maps. Of course, while scanning the probabilities from lowest to highest in the simulation, we obtain a continuous line. In the case of the chaotic maps, the dots that define that line do not go uniformly from end to end of the line, but they are scattered on top of the line as the control parameter of each map is scanned.

Looking at Fig. 3 we can appreciate that all the maps occupy parts of this curved line in the top part of the plane. None of the maps occupies the whole allowed curved line, and not all the maps occupy the exact same dots on the curved line. This is because the range of probabilities explored by each map is different, and also the maps do not explore the whole range of probabilities allowed by the constraints, despite satisfying these constraints among words, given by Eq. (4).

Because of the high symmetry imposed by the constraints in this region, there are only eight different groups of sorting arrays, which display eight different sections of the curved line (see all possibilities in ref. [23]).

It is worth noting that our numerical simulations, based on the probabilities, defines the allowed values on the plane, but it does not indicate which values of that line will be actually represented by each chaotic map. That is given by the combinations of probabilities that each map is covering, which is not the whole range. Remember that this numerical representation is based on relations among probabilities, and have nothing to do with any specific dynamical system. It shows the maximum set of possible values on the plane that the chaotic map can take, and it is a bound to the possible region where the map can be found on the plane.

For region III we impose the less restrictive constraint from Eq. (5), and plot all the possible values (see Fig. 6a). We scan the possible combinations of probabilities under this restriction: $0 \leq P_1 \leq 1$ and $1 \geq P_3 \geq 0$, maintaining $\sum_{i=1}^{5} P_i = 1$. Because of the more relaxed constraint, the possible landscape for this region is wider. Nevertheless, it can be appreciated how the projection of the logistic map is wrapped inside the allowed region of the simulation (Fig. 6b). It is worth remembering that the other chaotic maps under study show the same fingerprint on the complexity map, and therefore are also wrapped by the grid from the numerical simulations, as they all share the same constraints.

The logistic map, in its chaotic regime presents windows of periodicity. These windows correspond to more deterministic and symmetric dynamics which decrease PE and increase FIM. Those windows of periodicity can be spotted on the plane as dots (see Fig 6 d). Those dots lie at one of the boundaries of the allowed region defined by the simulation, indicated with arrows in the figure.

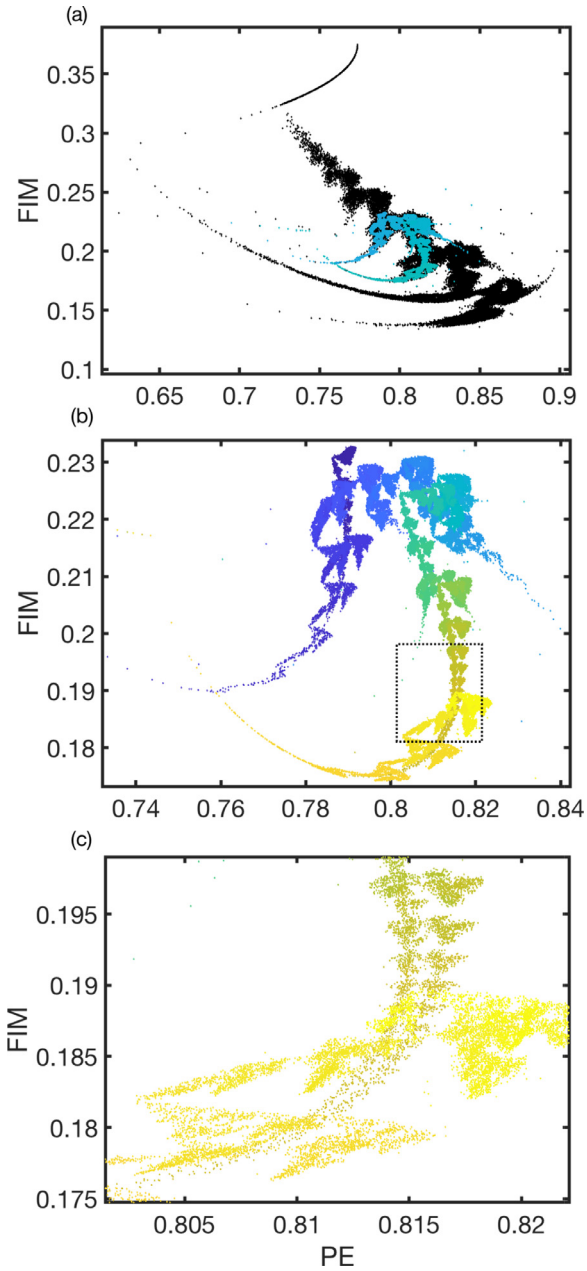

Fig. 7. Fisher-Shannon plane using SA* for the logistic map ($D = 3$). (a) shows the whole chaotic region of the logistic map. The portion in green is then zoomed in (b), where the fractal behaviour is evident. (c) zooms in the rectangle in (b). (For interpretation of the references to colour in this figure legend, the reader is referred to the web version of this article.)

5. Fractal behaviour unveiled by the Words-Fisher-Shannon plane

Sorting arrays SA* and SA† (505 and 307 in Ref. [23]) are two, out of the 720, that present more detail on the Fisher-Shannon plane than most of the others (see Fig. 2c, d). They both spread out the landscape of the maps on the plane, they do not present overlap of different regions, and they show different visual structure for different regions of the control parameter. By inspecting any of them (see Fig. 3 for SA*) one can appreciate certain repetition of the features that are not revealed by SA-Lehmer (See Fig. 1b). These repeated patterns suggest that this method can also unveil the self-similarity present in the logistic map.

For all the previous figures we used 10^4 or 10^5 points for a wide range of r values ($3.55 \leq r \leq 4.00$). In Fig. 7 we show the logistic map using 10^5 points in a reduced subset of r values ($3.70 \leq r \leq 3.75$), to see the finer details of the projection. Fig. 7a shows the wide-range logistic map projected on the plane. In Fig. 7b, the green section is zoomed in, where the fractal behaviour of the logistic map is noticeable. One can recognize the same pattern repeating, in the form of triangular structures that move down the plane, and get smaller and smaller as the control parameter r increases and the projection on the plane goes down in FIM. Fig. 7c zooms in into the rectangular section of Fig. 7b, to appreciate more detail.

The logistic map equation can be transformed into that of the Maldelbrot set, $z_{n+1} = z_n^2 + c$, by means of the change $z_n = r(\frac{1}{2} - x_n)$. From this, the self-similar behaviour of the logistic map can be explained through the fractality of the Mandelbrot set [26–28]. Nevertheless, it is remarkable that the words, which lose part of the time series information and only keep its temporal correla-

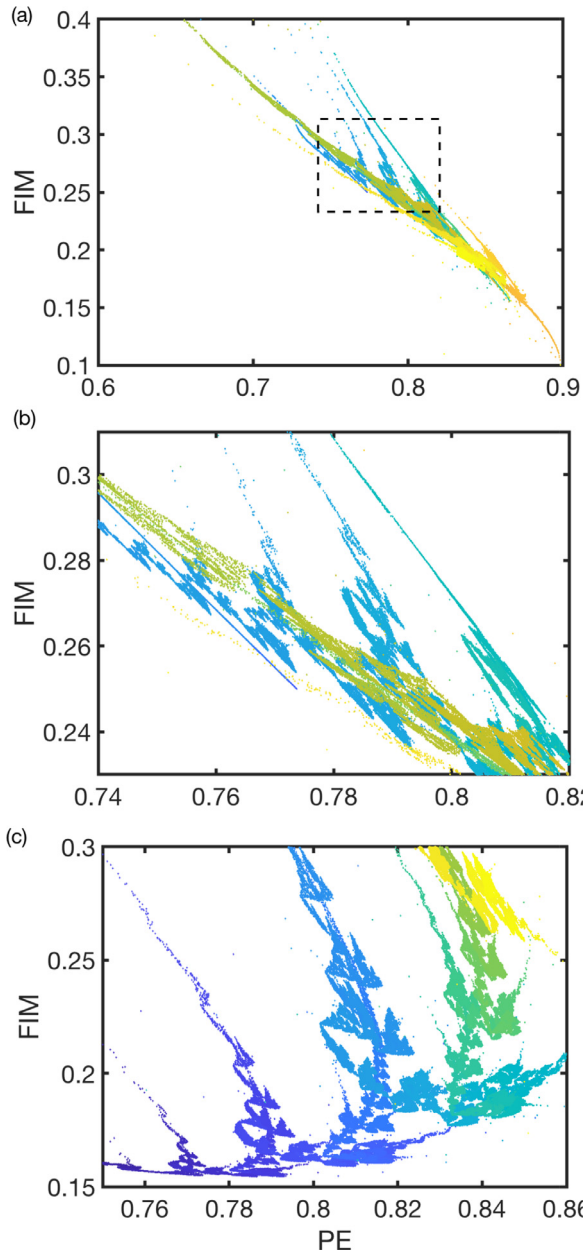

Fig. 8. Fisher-Shannon plane using SA-Lehmer for the logistic map. (a) Whole chaotic region of the logistic map. The dashed rectangle is zoomed in (b), where the fractal behaviour is clearer. (c) Fractal behaviour of the logistic map depicted with SA†.

tions, can also extract the self-similar essence through the Fisher-Shannon plane. Certainly, to appreciate this, one needs to compute a large density of r values for the projection. The sorting array can make a difference in this direction, as one can intuitively guess some self-similar behaviour from SA* (Fig. 2d) while none can be appreciated from SA-Lehmer (Fig. 2a).

Once we have seen that, for SA*, the ordinal-pattens-based Fisher-Shannon plane can detect fractal behaviour in these chaotic maps, we can explore other sorting arrays to look for self-similarity in the dynamics. Fig. 8a and b show the complexity plane using SA-Lehmer for 10^5 points for the logistic map. In it we can also appreciate a repeating pattern in the same range of parameters as in Fig. 7. The fact that we are using a different sorting array makes the repeating pattern be different in this case, but the underlying dynamical behaviour is clearly captured.

Similar results are found for other sorting arrays for the logistic map, and similar results are found for the other chaotic maps that present fractal behaviour through period-doubling route to chaos. Fig. 8c shows the same fractal behaviour, although with a different pattern on the plane, for the logistic map with SA†.

6. Conclusions

To summarize, we have investigated the relevance of sorting the words of dimension $D = 3$ and its impact on the Fisher-Shannon plane when computing PE and ordinal-patterns-based FIM. First we have found that interesting features that had been highlighted in recent research is robust to all sorting protocols: ordinal-patterns Fisher-Shannon projections help detect and classify different dynamical regions in chaotic maps. Also, the non-invertible maps studied present a common fingerprint on the plane when plotted with the same words order, independently of which order. The landscape of the fingerprint depends on the sorting array but it is the same for all the iterative maps considered.

Further, whilst higher order analysis ($D = 4, 5, 6, \dots$) is able to capture more features of the dynamics, a suitable choice of order for lower dimension ($D = 3$) can attain the same level of detail, while saving computational resources.

Looking at the dependence on the control parameter of the words probabilities we have extracted internal symmetries hidden in the chaotic dynamics of the maps. These symmetries are related to time inversion, and rotation symmetries, and impose constraints in the probabilities of the words, even in chaotic regions of the maps. These symmetries allow us to simulate the projection of the maps on the ordinal-patterns Fisher-Shannon plane. The simulations find the allowed region on the plane for the complex dynamics of any dynamical system with those symmetries. Therefore, given a new chaotic system that presents those symmetries we could determine the expected region where to locate it on the plane.

By exploring the complexity plane with more informative sorting arrays (such as SA* and SA†) finer details can be appreciated, such as self-similarity. Although fractal behaviour in period-doubling route to chaos systems is well known, it is remarkable how this technique can easily portray it. Also, the fractal behaviour is present independently of the sorting array. Of course, there are some SAs that capture those features in a clearer manner. We want to stress that, while some SAs can present the landscape of the system in a compressed, narrow region, with plenty of overlap, other SAs present the system more spread out. The latter makes it easier to characterize and distinguish different dynamics, which also applies also to detecting self-similarity.

One interesting aspect of this research that would be of interest to explore is to find a physical or mathematical generic method to determine which SA is optimum, i.e., presents a wider landscape or a broader range for FIM values. We have seen that this helps distinguish and characterize the complex dynamics. We have tried several criteria for find suitable SA protocols for $D = 3$, such as minimizing the distance to Gaussian white noise, or maximizing FIM. Although some of the criteria lead to SAs that seemed to be better than SA-Lehmer, none of them gave as much detail as that produced by SA* or SA†.

Another interesting aspect to explore is to generate a generalization to $D = 4$ of SA* or SA†. For $D = 4$ there are 24 words, and more than 6.2×10^{23} different sorting arrays. We have used SA-Lehmer to show that higher dimensions can extract more details of the complex dynamics. It is reasonable to think that there are SAs of $D = 4$ that can do a better job.

CRediT authorship contribution statement

David Spichak: Software, Formal analysis, Validation. **Andrés Aragoneses:** Visualization, Formal analysis, Supervision, Writing – original draft, Funding acquisition.

Declaration of Competing Interest

The authors declare that they have no known competing financial interests or personal relationships that could have appeared to influence the work reported in this paper.

CRediT authorship contribution statement

David Spichak: Software, Formal analysis, Validation. **Andrés Aragoneses:** Visualization, Formal analysis, Supervision, Writing – original draft, Funding acquisition.

Acknowledgements

AA would like to thank Egara for her support during the time of this research.

References

[1] Bradley E, Kantz H. Non-linear time series analysis revisited. Chaos 2015;25:097610.
[2] Politi A. Quantifying the dynamical complexity of chaotic time series. Phys Rev Lett 2018;118:144101.
[3] Toker D, Sommer FT, D'Esposito M. A simple method for detecting chaos in nature. Nat Comm Biology 2020;3.
[4] Daw CS, Finney CEA, Tracy ER. A review of symbolic analysis of experimental data. Rev Sci Instr 2003;74:915.
[5] Aragoneses A, Rubido N, Tiana-Alsina J, Torrent MC, Masoller C. Distinguishing signatures of determinism and stochasticity in spiking complex systems. Sci Rep 2013;3:1778.
[6] Vignat C, Bercher JF. Analysis of signals in the Fisher-Shannon information plane. Phys Lett A 2003;27:312.
[7] Olivares F, Plastino A, Rosso OA. Analysis of Shannon-Fisher information plane in time series based on information entropy. Phys Lett A 2012;376:1577–83.
[8] Olivares F, Plastino A, Rosso OA. Ambiguities in Bandt-Pompe's methodology for local entropic quantifiers. Physica A 2012;391:2518–26.
[9] Ravetti MG, Carpi LC, Goncalves BA, Freri AC, Rosso OA. Distinguishing noise from chaos: objective versus subjective criteria using horizontal visibility graph. PLoS ONE 2014;9:108004.
[10] Spichak D, Kupetsky A, Aragoneses A. Characterizing complexity of non-invertible chaotic maps in the Shannon-Fisher information plane with ordinal patterns. Chaos Solitons Fractals 2021;142:110492.
[11] Bandt C, Pompe B. Permutation entropy: a natural complexity measure for time series. Phys Rev Lett 2002;88:174102.
[12] Toomey JP, Kane DM. Mapping the dynamic complexity of a semiconductor laser with optical feedback using permutation entropy. Opt Express 2014;22:1713.
[13] Soriano MC, Zunino L. Time-delay identification using multiscale ordinal quantifiers. Entropy 2021;23:969.
[14] Bandt C. A new kind of permutation entropy used to classify sleep stages from invisible EEG microstructure. Entropy 2017;19:197.
[15] Aragoneses A, Carpi L, Tarasov N, Churkin DV, Torrent MC, Masoller C, Turitsyn SK. Unveiling temporal correlations characteristic of a phase transition in the output intensity of a fiber laser. Phys Rev Lett 2016;116:33902.
[16] Colet M, Aragoneses A. Forecasting events in the complex dynamics of a semiconductor laser with optical feedback. Sci Rep 2018;8:10741.
[17] Bandt C. Small order patterns in big time series: a practical guide. Entropy 2019;21:613.
[18] Zanin M, Guntekin B, Akturk T, Hanoglu L, Papo D. Time irreversibility of resting-state activity in the healthy brain and pathology. Front Physiol 2020;10:1619.
[19] Martin MT, Pennini F, Plastino A. Analysis of Shannon-Fisher information plane in time series based on information entropy. Phys Lett A 1999;256:173–80.
[20] Carpi L, Masoller C. Persistence and stochastic periodicity in the intensity dynamics of a fiber laser during the transition to optical turbulence. Phys Rev A 2018;97:023842.
[21] Fisher RA. Theory of statistical estimation. Proc Camb Phil Soc 1925;22:700–25.
[22] Frieden BR. Science from Fisher information: a unification. Cambridge University Press; 2004.
[23] 2021a. https://bit.ly/2XEqqvm.
[24] 2021b. https://bit.ly/2WPNIRZ.
[25] Gunther I, Pattanayak AK, Aragoneses A. Ordinal patterns in the duffing oscillator: analyzing powers of characterization. Chaos 2021;31:023104.
[26] Beck C. Physical meaning for maldelbrot and Julia sets. Physica D 1999;125:171–82.
[27] Isaeva OB, Kuznetsov SP, Ponomarenko VI. Mandelbrot set in coupled logistic maps and in an electronic experiment. Phys Rev E 2001;64:055201.
[28] Rani M, Agarwal R. Generation of fractals from complex logistic map. Chaos Solitons Fractals 2009;42:447–52.